Jurnal Teknologi

Full Paper

EXPERIMENTAL AND NUMERICAL STUDY ON THE BEHAVIOUR OF SILICA SAND SLOPE MODEL SUBJECTED TO SURCHARGE LOAD

Aina Syahirah Ahmad Ishak[a], Jestin Jelani[a]*, Soon Yee Wong[b], Zuliziana Suif[a], Ahmad Loqman Ahmad Mazuki[c]

[a]Department of Civil Engineering, Faculty of Engineering, National Defence University of Malaysia, 57000 Kuala Lumpur, Malaysia
[b]Department of Civil Engineering, Faculty of Science and Engineering, University of Nottingham Malaysia, 43500 Semenyih, Selangor, Malaysia
[c]Department of Electric and Electrical Engineering, Faculty of Engineering, National Defence University of Malaysia, 57000 Kuala Lumpur, Malaysia

Article history
Received
26 May 2023
Received in revised form
15 August 2023
Accepted
23 August 2023
Published Online
20 December 2023

*Corresponding author
jestin@upnm.edu.my

Graphical abstract

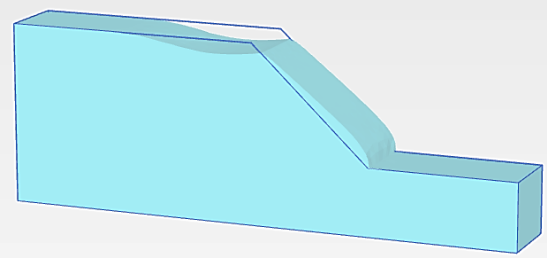

Abstract

Natural disasters such as landslides are becoming more frequent due to global warming. Because of the more frequent occurrences of natural disasters, there is an urgent need for researchers in geotechnical engineering to conduct slope stability analysis. This paper presents the findings of a laboratory experiment and numerical analysis of the behaviour of silica sand under static loading conditions. The laboratory experiment modelled a small-scale slope in a 500mm wide, 1000mm high and 1500mm long acrylic box. The numerical modelling in the experiment employed, Finite Element Modelling (FEM), Plaxis 3D, and the Hardening Soil Model (HSM). The researchers conducted a consolidated-drained (CD) triaxial compression test to determine the parameters of the silica sand. The FEM results are similar to the test results for the maximum loading conditions of 9.6kN/m^2. The experimental observation revealed that applying a surcharge load on the top of the slope surface resulted in deformation and bulging. These observations were consistent with and validated the experimental and numerical results. The results of this study will be used to investigate the application of a proposed prototype inclinometer sensor for slope monitoring technology.

Keywords: Hardening soil model, numerical modelling, Plaxis 3D, small-scale model, silica sand

Abstrak

Kejadian bencana alam seperti tanah runtuh semakin kerap disebabkan kesan pemanasan global. Disebabkan perkara ini, ia adalah penting untuk penyelidik kejuruteraan geoteknik melakukan analisis kestabilan cerun. Kertas kerja ini membentangkan keputusan uji kaji makmal dan analisis berangka kelakuan pasir silika di bawah bebanan statik. Uji kaji ini membina model cerun skala kecil dalam kotak akrilik dengan dimensi 500mm lebar, 1000mm tinggi dan 1500mm panjang. Pemodelan berangka uji kaji menggunakan perisian geoteknik, Model Unsur Terhingga (FEM), Plaxis 3D, dan Model Tanah Pengerasan (HSM). Parameter pasir silika untuk uji kaji ditentukan melalui ujian mampatan

terkukuh-salir (CD) tiga paksi/tripaksi. Keputusan FEM menunjukkan trend yang sama dengan keputusan ujian, untuk keadaan bebanan maksimum 9.6kN/m^2. Pemerhatian uji kaji menunjukkan bahawa mengenakan beban tambahan pada bahagian atas permukaan cerun akan menyebabkan ubah bentuk dan kesan pembonjolan. Pemerhatian ini selaras dengan dan mengesahkan keputusan uji kaji dan analisis berangka. Keputusan kajian ini akan digunakan dalam kajian berhubung aplikasi sensor inklinometer prototaip yang dicadangkan untuk teknologi pemantauan cerun.

Kata kunci: Model tanah pengerasan, pemodelan berangka, Plaxis 3D, model skala kecil, pasir silika

1.0 INTRODUCTION

One of the critical parameters in geotechnical engineering that is determined by the factor of safety, is slope stability analysis. The slope stability analysis has been receiving increasing attention and employed by researchers due to its crucial importance in ensuring stable and safe slopes in geotechnical engineering projects. The advances in modern technology facilitate soil testing and slope stability analysis of natural and man-made slopes, thus ensuring safe and cost-effective slope designs [1-3].

Numerical modelling for slope stability analysis is a powerful tool often adopted in geotechnical engineering projects [4, 5]. Numerical modelling techniques can provide solutions to problems that cannot be resolved using conventional procedures, such as complex geometry, non-linear behaviours, and in-situ stresses [1]. FEM using 3D finite element analysis is a popular tool for investigating complex geotechnical conditions [6].

The Plaxis 3D, a specialized three-dimensional finite element analysis computer program for analysing soil stresses and deformation was used to develop the 3D finite element model [7]. It has features to handle the critical parameters of complex geotechnical engineering structures [8, 9]. Among the constitutive models used in Plaxis 3D are the Mohr-Coulomb model (MC), the hardening soil model (HSM) and the hardening soil model with small-strain stiffness model.

Schanz *et al.,* developed the HSM which is an elasto-plastic second-order hyperbolic isotropic hardening model using the Plaxis software [10]. HSM exhibits material behaviour more realistically than the MC model concerning the non-linear stress-strain relationship with stress-dependent stiffness [11]. Moreover, it is regarded as one of the advanced soil constitutive modellings for studying the deformation problems of various geotechnical structures [12 - 20].

According to Chheng and Likitlersuang (2018), HSM can use the popular hyperbolic model developed by Duncan and Chang 1970 [21] to describe soft and stiff soils [4]. Schanz *et al.,* 1999 presented a detailed discussion of HSM [10]. Strength and stiffness are the critical parameters in slope deformation analysis. The soil model parameters using finite element methods are vital components for stress-deformation analyses of geotechnical structures [22].

The vertical strain, ε_1, and deviatoric stress, q, in the primary triaxial loading are characterized by a hyperbolic relationship in the HSM, where q_a is the asymptotic value of the deviatoric stress, and E_{oed}^{ref} is the reference soil tangent stiffness of the primary oedometer loading. The 50% of the ultimate deviatoric stress q_f, at a reference pressure, p_{ref} is represented as the confining stress-dependent stiffness modulus, E_{50}^{ref}. Another parameter in this model is E_{ur}^{ref}, which is the reference unloading/reloading stiffness modulus [22, 23].

The power law (m) represents the stress dependency level of soil stiffness, while φ' is the effective friction angle. In addition, ψ' is the effective dilation angle of the soil, and the ratio of the ultimate to asymptotic deviatoric stresses is the failure ratio, R_f [22].

This study determined the strength and stiffness of silica sand by conducting consolidated-drained triaxial compression tests. Furthermore, the study employed Plaxis 3D software to simulate and verify experimental results using the FEM software program. The paper presents and discusses the results from the laboratory tests and numerical analysis.

2.0 METHODOLOGY

2.1 Laboratory Testing

This study used fine and uniform dry silica sand and determined its physical properties following the British Standard (BS).

2.1.1 Sieve Analysis

The sieve analysis test followed BS 1377: Part 2:1990, while the classification of soil distribution was as per the British Soil Classification System (BS 5930.81). The sieve analysis test was conducted using a mechanical shaker shown in Figure 1.

Figure 1 Sieve analysis using a mechanical shaker

2.1.2 Soil Compaction Test

The soil compaction test followed BS 1377:1990: Part 4. It involved placing and compacting the soil sample in the mould by compacting each three layers of the soil sample with a 2.5 kg hammer for 25 blows, as shown in Figure 2.

(a) (b)

Figure 2 (a) and (b) Soil compaction

2.1.3 Consolidated-Drained Triaxial Test

This study measured the shear strength of the silica sand by conducting the CD triaxial compression test based on the British Standard (BS) BS:1377-8. The specimen is 50 mm in diameter and 100mm high. The cylindrical specimen was remoulded at the optimum moisture content. The typical triaxial system shown in Figure 3 consists of the pressure transducers, load cell, linear vertical displacement transducer (LVDT) and computer logging system to record and process the data.

Figure 4 shows the complete CD test equipment comprising the saturation, consolidation, and shearing stages for determining the drained parameters. Figure 4(a) shows the saturation stage using a 10kPa back-pressure saturation method. The consolidation stage shown in Figure 4(b) was consolidated at varying effective pressures of 50, 100 and 200kPa, while Figure 4(c) shows the shearing stage carried out after the consolidation stage. During the shearing stage, the drainage pipe was opened to allow any pore water pressure that had accumulated to dissipate.

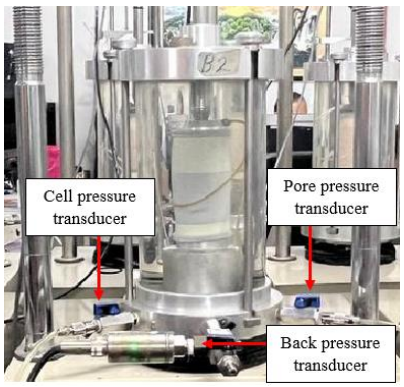

(a)

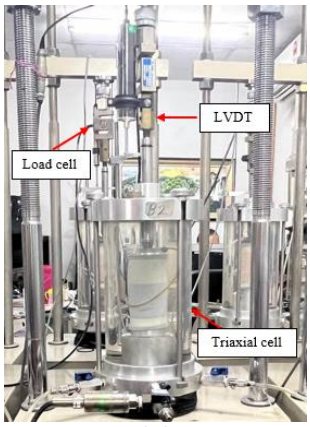

(b)

Figure 3 (a) and (b) The triaxial system

(a) (b) (c)

Figure 4 The three stages of the consolidated-drained triaxial compression tests are the (a) saturation stage (b) consolidation stage (c) shearing stage

2.2 Experimental Test

In the experimental test, the small-scale ground model was prepared in a 500 mm wide, 1500 mm long and 1000mm high acrylic box as shown in Figure 5. Figure 6 shows the compaction of silica sand in the acrylic box, where successive 100mm sand layers were compacted to achieve a height of 800mm, as shown in Figure 7. The relative density, or the ratio of compacted soil in the acrylic box to the soil compaction test, is 81%.

For each level of loading, a surcharge load of 8 kg was applied to the top of the soil slope model to initiate slope failure. The study used a 500mm long and 200 mm wide steel plate as a base to apply the surcharge load. In addition, several coloured marks using ink that have a distance of 30 mm from each other have been applied in this experiment as shown in Figure 7, to facilitate the observation of soil slope movement. The distance of ink is determined based on a grid attached to the surface of the acrylic box that has a dimension of 10 mm x 10 mm.

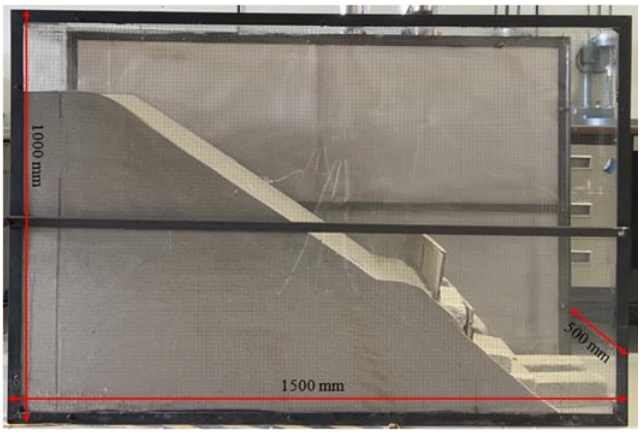

Figure 5 The dimensions of the acrylic box

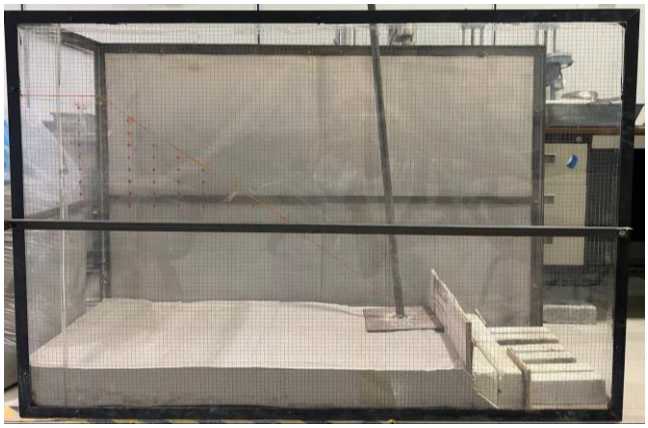

Figure 6 Compacting the soil slope model

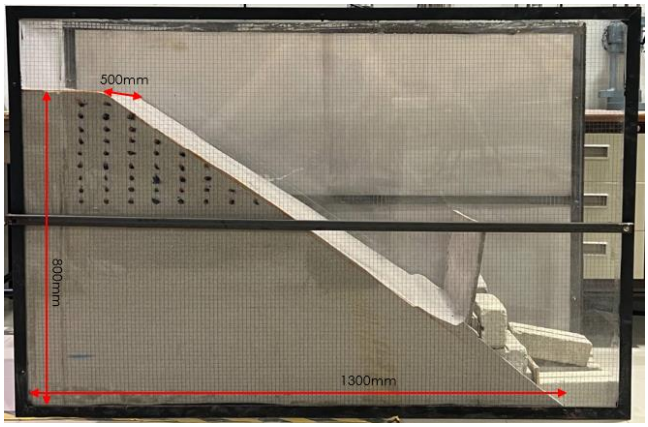

Figure 7 The dimensions of the soil slope model

2.3 Numerical Simulation using the Laboratory Test Results

The laboratory test results for the silica sand were used to perform numerical analysis using FEM and the Plaxis 3D software. The bottom boundary of the slope model has a fixed dimension of 2.0 m long, 0.8 m high and 0.5 m wide, and the ground surface was unrestrained from moving in all directions as shown in Figure 8. In order to prevent movements in the orthogonal directions, the vertical borders were fixed.

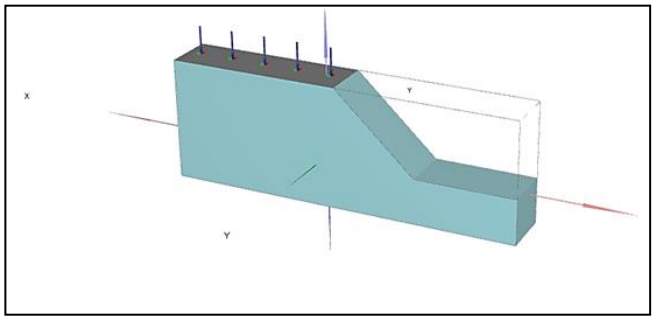

Figure 8 The slope model in Plaxis 3D software

In this study, each refinement's element size factor was automatically managed and the finite element models for the constructed slope used the medium mesh refinement. The numerical analysis for constructing the Plaxis model consists of three phases, namely the initial, excavation and surcharge phases. The initial phase was constructed by activating the materials, the excavation phase was analysed by deactivating the excavated soil volume, and the surcharge phase was carried out by applying the surcharge load on top of the soil surface.

3.0 RESULTS AND DISCUSSIONS

3.1 Aboratory Test

Figure 9 presents the particle size distribution curve, which shows that the soil consists of 0% gravel, 99.2% sand and 0.8% silt. The uniformity coefficient (C_u) and curvature coefficient (C_c) of 1.04 and 0.9 mean that the soil is uniformly graded sand.

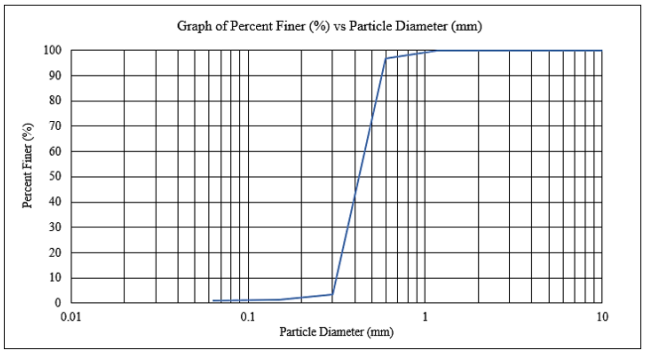

Figure 9 Sieve analysis results of silica sand

Figure 10 presents the silica sand's moisture content, w (%), and dry density, γ_d, determined through the standard proctor test. The silica sand has a maximum dry density of 15.33 kN/m^3 and 16.7% optimum moisture content.

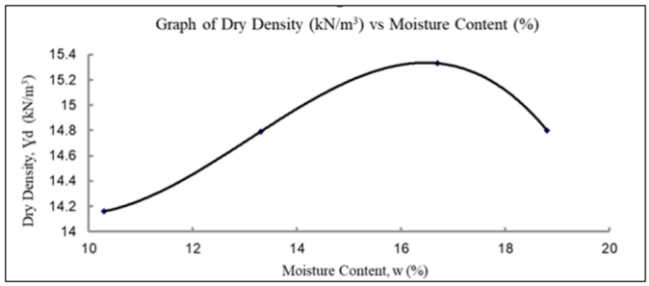

Figure 10 Graph of the silica sand's dry density, γd against moisture content, w (%)

Direct evaluations of the laboratory test results and parametric studies of curve fitting results were used to determined the input soil strength parameters of HSM for silica sand. Figures 11(a), (b) and (c) show the final conditions of the specimen after the CD triaxial test at varying confining pressures of 50kPa, 100kPa and 200kPa.

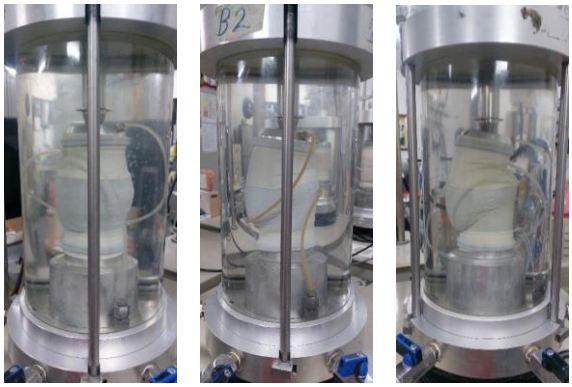

(a) (b) (c)

Figure 11 The specimens after failure at **(a)** 50kPa **(b)**100kPa **(c)** 200kPa

3.2 Stiffness Parameter

In the CD triaxial compression tests, Specimens A, B and C were subjected to varying confining pressures of 50kPa, 100kPa and 200kPa, respectively. Table 1 presents the effective minor and major principal stresses at failure for the three specimens, and Figure 12 shows the Mohr circle of the effective stress. The parameters obtained from the test results are cohesion, c, and angle of internal friction, φ.

Table 1 The shear strength results of silica sand

Specimen	Effective minor principal stress, σ'$_3$ (kPa)	Effective major principal stress, σ'$_1$ (kPa)
A	50	260.43
B	100	491.13
C	200	839.68

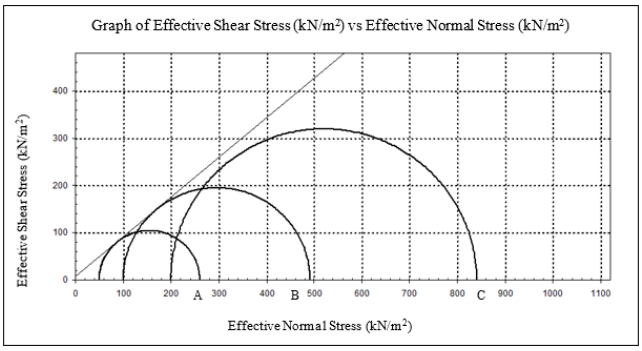

Figure 12 Mohr circle from the test result

The gradient from axial strain-volumetric strain curve shown in Figure 13 which gives the dilatancy angle, ψ, shows that the 50kPa confining pressure has a smaller dilatancy than the other confining pressures. Based on the confining pressure curve in Figure 12, the dilatancy rate, d value at 50kPa was 0.0236. The d value was used in Equation (1) to calculate the dilatancy angle, ψ [24].

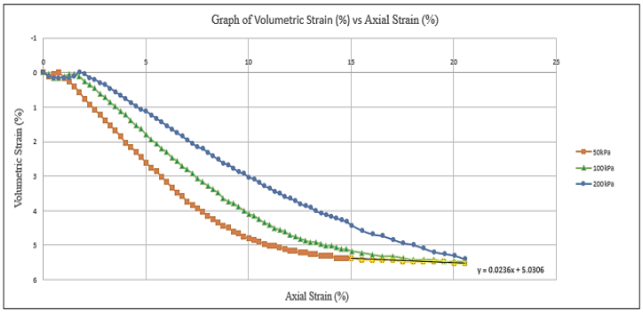

Figure 13 Determination of the dilatancy angle

$$\Psi = -\sin^{-1}(d/2\text{-}d) \quad (1)$$

The plastic soil stiffness parameter, E_{50}^{ref}, was determined from the CD triaxial test. Figure 14 shows the deviatoric stress-strain curve for the three confining pressures, and Figures 15(a), (b) and (c) show the determination of the E_{50}^{ref} for specimens at confining pressures of 50kPa, 100kPa and 200 kPa, that shows softening behaviours. The E_{50}^{ref} for Specimens A, B and C are 28404kPa, 32138kPa and 54929kPa.

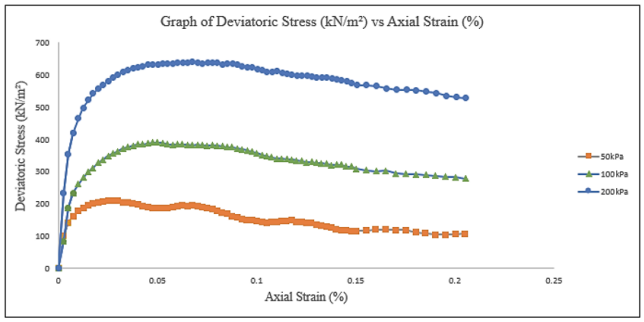

Figure 14 The stress-strain curve

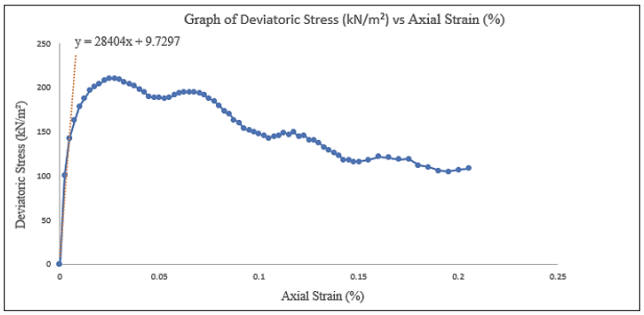

(a)

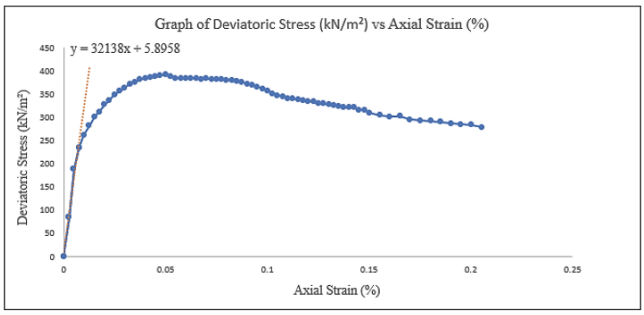

(b)

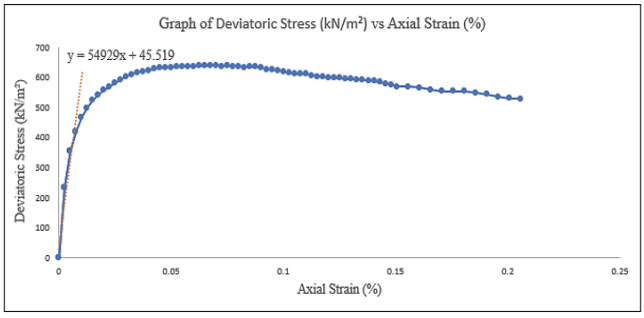

(c)

Figure 15 Determination of the E_{50} moduli at **(a)** 50kPa, **(b)** 100kPa, and **(c)** 200kPa

Figure 16 shows the determination of m value based on the slope inclination relationship between ln $[(\sigma'^3 + c\ cot\Phi)/(100 + c\ cot\Phi)]$ and ln E_{50} [25]. The value for m is 0.5.

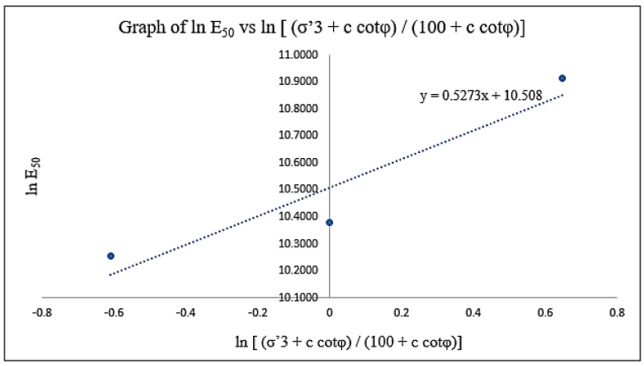

Figure 16 Determination of the stress dependency level of the soil stiffness (m) parameter

The secant stiffness, E_{50}^{ref} is derived from Equation (2) and the results are tabulated in Table 2 [26]. The final E_{50}^{ref} is determined from the average values of a total of three soil testing.

$$E_{50} = E_{50}^{ref}\ [(\sigma'^3 + c\ cot\Phi)/(100 + c\ cot\Phi)]^m \quad (2)$$

Table 2 Secant stiffness, E_{50}^{ref}

σ'_3 (kPa)	E_{50} (kPa)	$[(\sigma'^3 + c\ cot\Phi)/(100 + c\ cot\Phi)]^m$	E_{50}^{ref} (kPa)
50	28404	0.737	38540.03
100	32138	1.000	32138.00
200	54929	1.383	39717.28
Average			36798.44

The value of v, R_f and p^{ref} were obtained from Plaxis manual with value of 0.2, 0.9, 100kN/m^2, while K, E_{oed}^{ref} and E_{ur}^{ref} were obtained from equations of 1-sinφ, $E_{50}^{ref}/1.25$, and $3E_{50}^{ref}$ respectively [11, 20, 24]. Table 3 presents the description and input strength parameters of HSM obtained from the CD triaxial tests results.

Table 3 The parameters of the HSM for the silica sand

Parameter	Value	Unit
E_{50}^{ref}	36798	kN/m^2
E_{oed}^{ref}	29438	kN/m^2
E_{ur}^{ref}	110394	kN/m^2
v_{ur}	0.2	-
p^{ref}	100	kN/m^2
K_0	0.3572	-
c	8	kN/m^2
φ	40	degree(°)
γ	15.33	kN/m^3
ψ	0.7	degree(°)
m	0.5	-
R_f	0.9	-

3.3 Validation of Soil Properties with Previous Studies

Table 4 compares the soil properties determined through laboratory tests with those from previous studies based on the HSM parameters. The E_{50}^{ref} and E_{oed}^{ref} stiffness parameters range between 16MPa and 26MPa, and the values for E_{ur}^{ref} range between 48MPa and 78MPa.

Based on the previous results, the cohesion and friction angle properties vary from 0.06 to 9 and 29 to 36 degrees. The findings of this study consisted with previous studies.

Table 4 The soil properties from previous studies

Reference	Wang *et al.* [27]	Momemi *et al.* [28]	Momemi *et al.* [28]	Zheng *et al.* [29]
E_{50}^{ref} (MPa)	17.5	15.99	25.86	50
E_{oed}^{ref} (MPa)	17.5	15.99	25.86	50
E_{ur}^{ref} (MPa)	70	47.97	77.58	150
v_{ur}	0.2	0.2	0.2	-
K_0	0.4179	0.49	0.51	-
c (kN/m²)	8.6	0.06	0.08	1
Φ (°)	35.6	30.5	29	35
Ψ (°)	5.6	-	-	-
m	0.336	0.5	0.5	-
γ (kN/m³)	17.9	19.5	19.63	-

3.4 Numerical Analysis

The numerical analysis used the Plaxis 3D geotechnical software with HSM parameters to numerically model and simulate the physical slope model failure.

Figures 17(a)-(c) show the results of the soil numerical analysis using Plaxis 3D software. Figure 17(a) shows the state of the soil slope model, where there is more movement at the top of the slope and on the inclined surface. The red area in Figures 17(b) and (c) are the most critical when applying the surcharge load. The numerical analysis gave a factor of safety of 3.61.

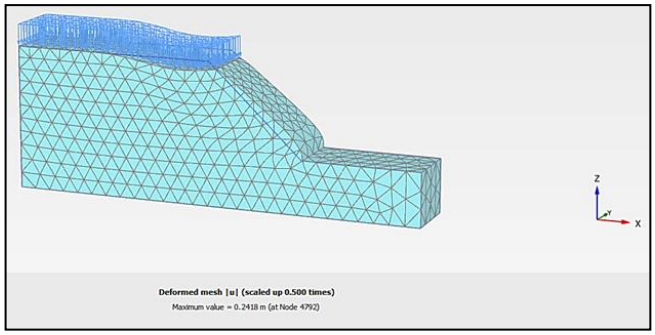

(a)

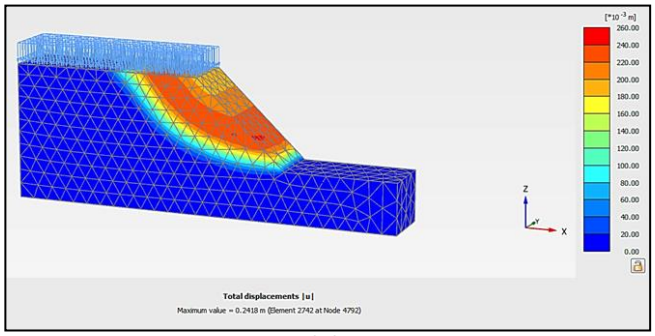

(b)

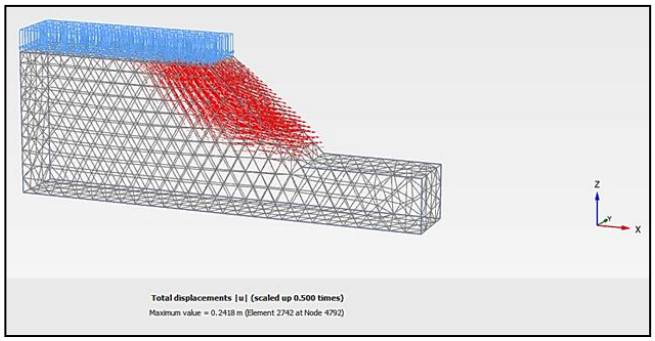

(c)

Figure 17 The finite elements given by Plaxis, 3D for (a) mesh deformation (b) contour deformation, and (c) location of the critical deformation

3.5 Verification of the Experimental and Numerical Results

This study compared the experimental and numerical results. Figure 5 shows the initial state of the soil slope model with a dimension of 500mm wide, 1500mm long and 800mm high. Figure 7 shows the soil slope model coloured with markers to facilitate observation of whether the applied load caused any soil movements.

Figure 18 shows the experiment was conducted with load values of 9.6kN/m². Figure 18(a) and (b) show the experimental results and have been compared with the numerical analysis shown in Figure 18(c). The soil movement in the experimental and numerical slope model occurred primarily on top of the slope, and there was bulging near the slope surface. Figure 18(b) shows that the maximum soil movement based on the vertical axis of the experimental results is 2cm, whereas the numerical analysis gave a maximum soil movement of 3cm, as shown in Figure 18(c).

(a)

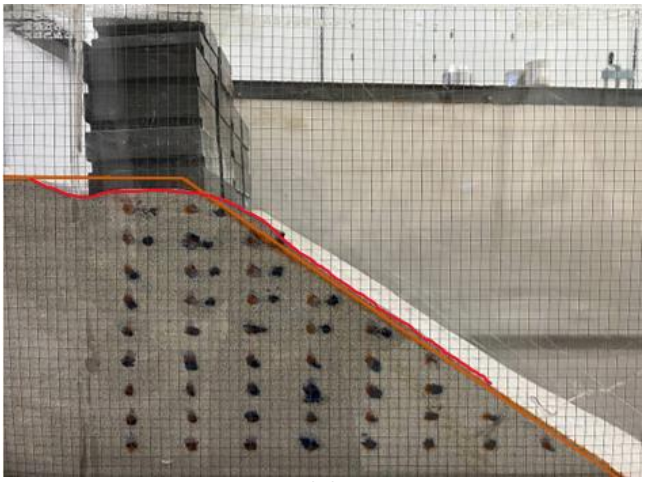

(b)

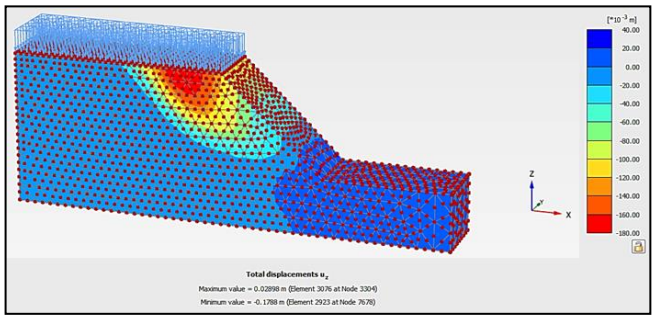

(c)

Figure 18 The results based on the (a) experimental results (b) soil displacement after failure, and (c) Plaxis 3D analysis

4.0 CONCLUSION

This study performed numerical analysis using FEM to simulate the experimental results and verify them using Plaxis 3D program. The soil slope behaviour was also described using the hardening soil parameters obtained from the CD triaxial tests. The soil compaction results showed that the silica sand has a maximum dry density of 15.33 kN/m^3, optimum moisture content of 16.7%, and 12.47kN/m^3 relative density. The shear strength parameters for c, φ, ψ and m were 8kPa, 40°, 0.7° and 0.5, and the stiffness parameter, E_{50}^{ref}, is 36798kPa. This study adopted the E_{oed}^{ref}, E_{ur}^{ref}, v_{ur}, p^{ref}, R_f and K_0 values recommended in the Plaxis manual. The findings from this study for HSM parameters of silica sand can provide a beneficial guide to carry out further studies on similar soil types. Furthermore, analysis of the numerical and experimental results revealed that the load application caused similar bulging on the top surface of the slope. In summary, slope stability analysis with numerical modelling of advanced constitutive soil models is beneficial in geotechnical analyses and provides a better understanding of soil behaviour.

Conflicts of Interest

The author(s) declare(s) that there is no conflict of interest regarding the publication of this paper.

Acknowledgement

The authors wish to express their gratitude to the National Defence University of Malaysia for funding and supporting this project under the grant with project code PS0056-UPNM/2022/GPPP/TK/24.

References

[1] Salunkhe, D. P., Bartakke, R. N., Chvan, G. and Kothvale, P. R. 2017. An Overview on Methods for Slope Stability Analysis. *International Journal of Engineering Research & Technology*. 6(3): 528–535.

[2] Ishak, A. S. A., Jelani, J., Dardin, S. M. F. S. M., Rashid, Z. A. and Suif, Z. 2023. Concept Development of Inclinometer for Real-time Data Collection in Slope Movement Detection. *Journal of Engineering Science and Technology*. 18(1): 132-144.

[3] Jelani, J., Hah, M. S. A., Mohd Daud, M. N., Ahmad, N., Othman, M., and Wan Mohamed Sabri, W. M. S. 2021. Stability Analysis of a Man-made Slope: A Case Study on the UPNM Campus, Sg Besi, Kuala Lumpur. *Environmental Science and Engineering*, 39-46. Doi: https://doi.org/10.1007/978-3-030-75278-1_4.

[4] Chheng, C. and Likitlersuang, S. 2018. Underground Excavation Behaviour in Bangkok using Three-dimensional Finite Element Method. *Computers and Geotechnics*. 95: 68-81. Doi: https://doi.org/10.1016/j.compgeo.2017.09.016.

[5] Ikeagwuani, C. C. and Nwonu, D. C. 2019. Emerging Trends in Expansive Soil Stabilisation: A Review. *Journal of Rock Mechanics and Geotechnical Engineering*. 11(2): 423-440. Doi: https://doi.org/10.1016/j.jrmge.2018.08.013.

[6] Wolf, T. K., Rasmussen, K. L., Hansen, M., Roesen, H. R. and Ibsen, L. B. 2013. Assessment of p-y Curves from Numerical Methods for a non-Slender Monopile in Cohesionless Soil. Technical Memorandum. Aalborg University.

[7] PLAXIS 3D-Reference Manual. 2020. Bentley.

[8] Abdelaziz, A., Hafez, D. and Hussein, A. 2017. The Effect of Pile Parameters on the Factor of Safety of Piled-slopes using 3D Numerical Analysis. *HBRC Journal*. 13(3): 277-285. Doi: https://doi.org/10.1016/j.hbrcj.2015.06.002.

[9] Al-Dawoodi, B. A., Rahil, F. H. and Waheed, M. Q. 2021. Numerical Simulation of Shallow Foundation Behavior Rested on Sandy Soil. *IOP Conference Series: Earth and*

Environmental Science. 856(1): 1-10. Doi: https://doi.org/10.1088/1755-1315/856/1/012042.
[10] Schanz, T., Vermeer, P. A. and Bonnier, P. G. 1999. The Hardening Soil Model: Formulation and Verification. *Beyond 2000 in Computational Geotechnics*. 281-296.
[11] Ukritchon, B., Ouch, R., Pipatpongsa, T. and Khosravi, M. H. 2018. Investigation of Stability and Failure Mechanism of Undercut Slopes by Three-dimensional Finite Element Analysis. *KSCE Journal of Civil Engineering*. 22(5): 1730-1741. Doi: https://doi.org/10.1007/s12205-017-2011-x.
[12] Morrison, K. F., Harrison, F. E., Collin, J. G., Dodds, A. M. and Arndt, B. 2006. Shored Mechanically Stabilized Earth (SMSE) Wall Systems Design Guidelines (No. FHWA-CFL/TD-06-001). United States. Federal Highway Administration. Central Federal Lands Highway Division.
[13] Obrzud, R. F. 2010. On the Use of the Hardening Soil Small Strain Model in Geotechnical Practice. *Numerics in Geotechnics and Structures*. 16: 1-17.
[14] Singh, V. P. and Sivakumar Babu, G. L. 2010. 2D Numerical Simulations of Soil Nail Walls. *Geotechnical and Geological Engineering*. 28: 299-309.
[15] Surarak, C., Likitlersuang, S., Wanatowski, D., Balasubramaniam, A., Oh, E. and Guan, H. 2012. Stiffness and Strength Parameters for Hardening Soil Model of Soft and Stiff Bangkok Clays. *Soils and Foundations*. 52(4): 682-697.
[16] Ruiz, J. F. and Rodríguez, L. M. 2015. Application of an Advanced Soil Constitutive Model to the Study of Railway Vibrations in Tunnels through 2D Numerical Models: A Real Case in Madrid (Spain). *Journal of Construction*. 14(3): 53-61.
[17] Gaur, A. and Sahay, A. 2017. Comparison of Different Soil Models for Excavation using Retaining Walls. *SSRG International Journal of Civil Engineering*. 4(3): 43-48.
[18] Skels, P. and Bondars, K. 2017. Applicability of Small Strain Stiffness Parameters for Pile Settlement Calculation. *Procedia Engineering*. 172: 999-1006.
[19] Likitlersuang, S., Chheng, C., Surarak, C. and Balasubramaniam, A. 2018. Strength and Stiffness Parameters of Bangkok Clays for Finite Element Analysis. *Geotechnical Engineering Journal of the SEAGS & AGSSEA*. 49(2): 1-7.
[20] Wu, J. T. H. and Tung, S. C.-Y. 2020. Determination of Model Parameters for the Hardening Soil Model. *Transportation Infrastructure Geotechnology*. 7(1): 55-68. Doi: https://doi.org/10.1007/s40515-019-00085-8.
[21] Duncan, J. M. and Chang, C. Y. 1970. Nonlinear Analysis of Stress and Strain in Soils. *Journal of the Soil Mechanics and Foundations Division*. 96(5): 1629-1653.
[22] Sobhey, M., Shahien, M., el Sawwaf, M. and Farouk, A. 2021. Analysis of Clay Slopes with Piles Using 2D and 3D FEM. *Geotechnical and Geological Engineering*. 39(3): 2623-2631. Doi: https://doi.org/10.1007/s10706-020-01627-5.
[23] Spagnoli, G., Doherty, P., Murphy, G. and Attari, A. 2015. Estimation of the Compression and Tension Loads for a Novel Mixed-In-Place Offshore Pile for Oil and Gas Platforms in Silica and Calcareous Sands. *Journal of Petroleum Science and Engineering*. 136(2015): 1-11. Doi: https://doi.org/10.1016/j.petrol.2015.10.032.
[24] Saleh, S., Mohd Yunus, N. Z., Ahmad, K. and Mat Said, K. N. 2021. Numerical Simulation with Hardening Soil Model Parameters of Marine Clay obtained from Conventional Tests. *SN Applied Sciences*. 3(156): 1-13. Doi: https://doi.org/10.1007/s42452-020-04115-w.
[25] Obrzud, R. F., and Truty, A. 2018. The Hardening Soil Model-A Practical Guidebook. Z Soil. PC 100701 Report. Switzerland: Zaca Service Ltd.
[26] El Kahi, E., Deck, O., Khouri, M., Mehdizadeh, R., and Rahme, P. 2020. A New Simplified Meta-model to Evaluate the Transmission of Ground Movements to Structures Integrating the Elastoplastic Soil Behavior. *Structures*. 23: 324-334.
[27] Wang, F., Han, J., Corey, R., Parsons, R. L., and Sun, X. 2017. Numerical Modeling of Installation of Steel-Reinforced High-Density Polyethylene Pipes in Soil. *Journal of Geotechnical and Geoenvironmental Engineering*. 143(11): 1-9. Doi: https://doi.org/10.1061/(ASCE).
[28] Momeni, E., Maizir, H., Gofar, N., and Nazir, R. 2013. Comparative Study on Prediction of Axial Bearing Capacity of Driven Piles in Granular Materials. *Jurnal Teknologi*. 61(3): 15-20.
[29] Zheng, A. 2018. Finite Element Analysis on Bearing Capacity of Post-Grouting Bored Pile with the HS-Small Model and the HS Model. *IOP Conference Series: Earth and Environmental Science*. 189(2): 1-6. Doi: https://doi.org/10.1088/1755-1315/189/2/022087.